Editor,
EarthArxiv,

Please see below details as the coversheet details requested during the pre-print submission process.

Topic: Magma solidification effects during sill emplacement: insights from laboratory experiments

Authors: Uchitha N. Arachchige[1], Alexander R. Cruden[1], Roberto Weinberg[1],

Affiliation: [1]School of Earth, Atmosphere and Environment, Monash University, 9 Rainforest Walk, Clayton, VIC 3800, Australia

I hereby confirm that this manuscript is a non-peer reviewed paper submitted to the EartArxiv. It has been submitted to the Earth and Planetary Science Letters journal and is under review now.

Please address all correspondence concerning this manuscript to me at uchitha.nissankaarachchige@monash.edu.

Thank you for your consideration of this manuscript.

Sincerely,

Uchitha Nissanka Arachchige,

School of Earth, Atmosphere and Environment
Monash University
9 Rainforest Walk
Clayton, VIC 3800
Australia

M: +61(0)453008250
E: uchitha.nissankaarachchige@monash.edu

Magma solidification effects during sill emplacement: insights from laboratory experiments

Uchitha N. Arachchige[1], Alexander R. Cruden[1], Roberto Weinberg[1],

[1]School of Earth, Atmosphere and Environment, Monash University, 9 Rainforest Walk, Clayton, VIC 3800, Australia

ABSTRACT

Igneous sills and interconnected sill complexes transport magma both vertically through the Earth's crust and laterally over potentially long distances. Although cooling and solidification of magma are acknowledged to play a major role in the propagation and emplacement of sills, their contributions to sill formation remain poorly understood. Here, the effects of solidification on sill propagation dynamics and the resulting intrusion morphologies are investigated using scaled laboratory experiments. Hot coconut oil (magma analogue) that solidifies during emplacement is injected as a sill into a colder, layered, solid visco-elasto-plastic gel (Laponite RD®, host rock analogue). Molten coconut oil is injected directly into the horizontal interface between two Laponite RD® layers to facilitate sill formation. The injection temperature and volumetric flow rate of the coconut oil are systematically varied between experiments in order to vary the degree of solidification. When solidification effects are relatively weak (high injection temperatures), sill propagation is continuous and forms penny-shaped intrusions that later turn into saucer-shaped sills with marginal segmentation. Conversely, when solidification effects are intermediate to relatively strong (low injection temperatures), sills develop complex elongate morphologies that lengthen parallel to the long-axis of the magma flow direction. Such sills also form in a discontinuous manner and propagate in pulses by growth of discrete marginal lobes, representing periods of tip arrest due to freezing, followed by growth of new lobes at the sill margins. A striking morphological feature that occurs in experiments with intermediate to relatively strong solidification effects is the presence of internal flow channels

within sills, which can be: (a) thermally controlled, long-lived channels in intermediate solidification experiments; or (b) structurally controlled, randomly oriented short-lived channels in strong solidification experiments. Our experimental findings are consistent with field and seismic observations of sill geometries, and they highlight that the relative degree of solidification during magma emplacement controls both how sills propagate and their internal flow dynamics.

1. INTRODUCTION

Magma is transported vertically through the Earth's crust via dykes and up to hundreds of kilometres horizontally in sills (Miles and Cartwright, 2010; Magee et al., 2016a; Muirhead et al., 2016). Magma cools during transport leading to orders of magnitude increases in its viscosity and eventual solidification (e.g., Currier and Marsh, 2015). Such large variations in magma viscosity makes it a key parameter governing the emplacement and the dynamics of igneous intrusions. However, changes in viscosity are challenging to simulate in laboratory and numerical experiments due to their dependence on temperature, crystallinity and melt composition. Therefore, the majority of previous analogue and numerical models of magma intrusion have adopted an isothermal approximation, and the temperature-dependant effects of magma cooling and solidification during emplacement of dykes and sills are often ignored.

Early studies on the effects of magma cooling and solidification focused on modelling the morphology and dynamics of lava flows (Fink and Griffiths, 1990; Griffiths and Fink, 1993; Stasiuk and Jaupart, 1997; Robertson and Kerr, 2012). Theoretical (Pollard et al., 1982; Bruce and Huppert, 1989; Lister and Dellar, 1996; Bolchover and Lister, 1999) and numerical (Rubin, 1993) studies of the effects of magma solidification during emplacement of dykes and sills are limited to two-dimensions. Most three-dimensional (3D) magma intrusion laboratory experiments have so far used isothermal magma analogues (e.g., Kavanagh et al., 2006; Galland et al., 2009; Arachchige et al., 2022) due to practical challenges in using analogue

materials capable of simulating magma solidification. Using gelatine and molten paraffin wax as crustal rock and magma analogues, respectively, Taisne and Tait (2011) were the first to experimentally investigate 3D solidification effects during the propagation of dykes. Their results show that solidification has a strong impact on dyke dynamics: when solidification effects are strong, experimental dykes display intermittent, step-wise propagation; and they propagate continuously when solidification effects are weak. More recent experimental studies of solidifying dykes (Chanceaux and Menand, 2014) and sills (Chanceaux and Menand, 2016) using visco-elastic gelatine (crustal analogue) and Newtonian vegetable oil (magma analogue) also observed discontinuous, step-like propagation and the formation of lobate segments at non-planar intrusion fronts. Currier and Marsh (2015) also modelled laccolith emplacement and documented complex emplacement styles and morphologies, which they attributed to solidification at the leading edge of magma-filled cracks. A study by Pansino et al. (2019) in which warm liquid gelatine was injected into cold, solid gelatine showed, for the first time, the existence of channelized dykes and conduit geometries within intrusions.

It is widely accepted that horizontal transport of magma is critical in magma plumbing systems, such as those with volcanoes that are laterally offset from their reservoirs (Hansen and Cartwright, 2006; Gudmundsson, 2011; Tibaldi, 2015; Magee et al., 2016b; Muirhead et al., 2016) and in giant radiating dike swarms (Ernst et al., 1995; Macdonald et al., 2010). It has also been suggested that interconnected sill complexes can facilitate lateral subsurface flow over hundreds to thousands of kilometres (Ernst et al., 1995; Macdonald et al., 2010; Muirhead et al., 2012; Magee et al., 2016b). Therefore, knowledge on the formation mechanisms and propagation dynamics of solidifying sills are key to understand the petrography and morphology of sills at both the intrusion and magma plumbing system scales.

Recent field, experimental and 3D seismic reflection data analyses of shallow igneous intrusions have shown that sills have complex geometries with highly segmented margins

consisting of lobes and fingers, which contrast with the conventional view of simple planar intrusions (Thomson and Hutton, 2004; Miles and Cartwright, 2010; Arachchige et al., 2022; Köpping et al., 2022). In isothermal experiments of analogue magma emplacement into a layered visco-elasto-plastic crustal analogue (Laponite RD® gel), Arachchige et al. (2022) modelled the formation of saucer-shaped sills with complex marginal segmentation. They showed that: (1) the transition from an inner flat sill to an outer inclined sheet occurs when the sill radius to overburden depth ratio is between 0.5 and 2.5; (2) the inclination of the outer inclined sheets varies from 15° to 25°; and (3) the transition from an inner flat sill to an outer inclined sheet is controlled by the ratio of the Young's modulus between the host material layers. Arachchige et al. (2022) concluded that the geometry of natural sills is compatible with brittle-elastic fracture mechanisms operating at the intrusion scale, while complex marginal segmentation is most likely linked to visco-plastic instabilities occurring at the crack-tip scale, possibly supported by the low fracture surface energy of the host material.

Isothermal analogue experiments of dykes by Kavanagh et al. (2018) have also shown the development of complex internal flow patterns (i.e., channelization). Pansino et al. (2019) observed similar channelization within solidifying dykes, which formed due to the internal circulation of heat between the dyke centre and its margins. Understanding this channelization or flow focusing is important in a number of magmatic environments, such as centralized vents in fissure eruptions (Fukushima et al., 2010; Jones et al., 2017), hot spot volcano zones (Leslie et al., 2004; Lundgren et al., 2013), dyke and sill complexes (Holness and Humphreys, 2003) and ore deposition (e.g., orthomagmatic sulphide deposits) in narrow, tube-like intrusions and in channels within sills (Barnes et al., 2016). To the best of our knowledge, such internal channelization has not yet been observed in either isothermal or solidifying sill experiments. Therefore, the internal structure in and overall morphology of sills that may result from cooling and solidification effects are currently poorly constrained and many questions remain to be

answered, such as, what is the impact of solidification on the style of sill propagation and the development of marginal segmentation? And, can magma flow form channels within solidifying sills?

Answers to these questions can potentially be found by carrying out 3D experiments that simulate injection of a hot, temperature-dependant viscous fluid into a cold visco-elastic-plastic host material, and by analysing the geometry and internal flow dynamics of the resulting intrusions and the associated host rock deformation. Here, we document the results of laboratory experiments in which hot coconut oil (the magma analogue) is injected into layered, cold visco-elastic-plastic Laponite RD® (LRD) gels, simulating the upper crust. Our main objectives are to: (a) understand the effect of cooling and solidification on the formation of sills emplaced into upper crustal host rocks with complex rheology; and (b) explore emplacement dynamics and intrusion morphologies as a function of the degree and rate of magma solidification.

2. MODEL SETUP, MATERIALS, SCALING, EXPERIMENT MONTORING AND ANALYSIS

2.1. Model setup

The experimental setup comprises a plexiglass tank (40 cm x 40 cm x 40 cm) filled with two layers of Laponite RD® (LRD) gel (crustal analogue) into which the sill is injected (Fig. 1). In all experiments, the upper (L1) and lower (L2) LRD layers have the same Laponite® concentration, X = 4 wt. % and the same Young's modulus, E = ~10^5 Pa (Arachchige et al., 2021). Molten coconut oil (magma analogue) is injected horizontally into the interface between the LRD layers at a volumetric flow rate, Q of 1 to 5 m^3 s^{-1} via a needle at the side of the tank, fed by a temperature- and flow rate-controlled digital syringe pump. The temperature of the coconut oil is set by a heating jacket around the syringe pump reservoir coupled with a thermal controller, and the initial temperature of the LRD is obtained by placing

the tank in a fridge for several hours before each experiment. The tank is then taken out of the fridge and left to warm up until it reaches the desired internal temperature, which is measured with a thermocouple probe. The temperature of the injecting fluid and Laponite gel in the tank are periodically monitored during the experiments. Propagation of the experimental sill is monitored by high resolution DSLR cameras (Fig. 1). The analogue magma injection temperature T_i and the volumetric flow rate Q are controlled independently, and kept constant during each experiment. These two parameters are varied between experiments in order to control the degree of analogue magma solidification.

2.2. Crustal host rock and magma analogue materials

The upper crustal host rock analogue comprises Laponite RD® (LRD), a gel-forming grade of synthetic smectite clay manufactured by BYK Additives and Instruments (2014). LRD gels are useful as upper-crustal rock analogues in laboratory experiments (Bertelsen et al., 2018; Arachchige et al., 2021) due to their visco-elasto-plastic rheology and because their Young's modulus can be controlled by varying their concentration in water and curing time (Arachchige et al., 2021). When mixed with water, LRD forms a transparent gel, which is similar to gelatine but is colourless and more transparent. Due to its chemical and biological stability, LRD gels are easy to handle and very versatile for use in laboratory experiments. LRD gel has lower surface energy values (24 - 44 mJ/m^2; (Norris et al., 1993) compared to other frequently used host rock analogue gels such as gelatine (1 J/m^2; (Kavanagh et al., 2013). This ensures that surface tension dynamics are minimized.

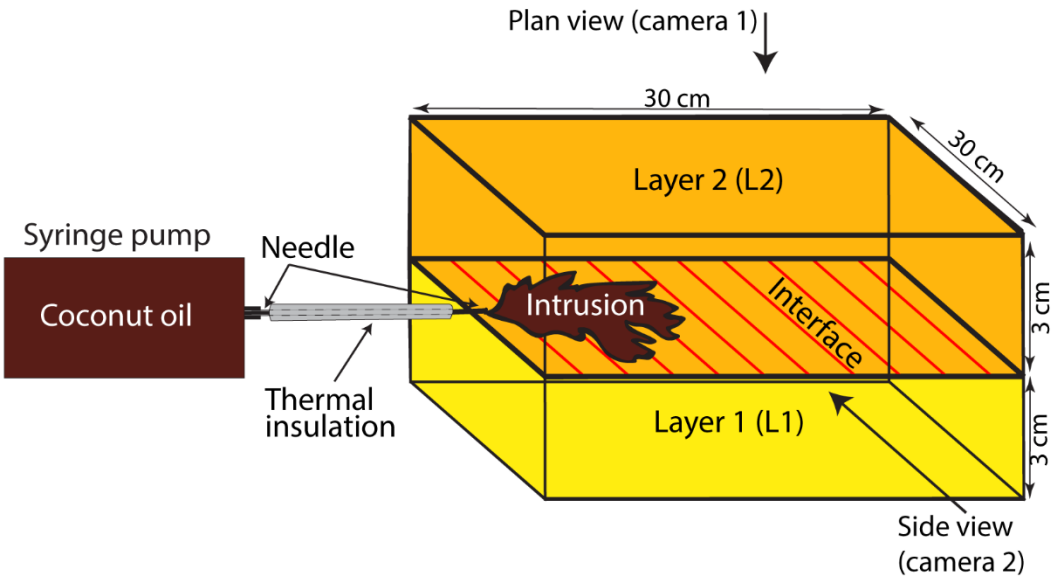

Figure 1. Schematic diagram of the experimental setup used in this study. A pressure and temperature control syringe pump injects coconut oil horizontally via a needle into two-layer Laponite RD® gel. Two high-resolution DSLR cameras capture the geometric details of sill propagation from top and side views.

We use coconut oil (extra virgin) as the magma analogue due to its liquid-solid transition upon cooling and non-reactive stability with LRD. The liquid-solid transition was measured with an Anton Parr MCR 301 rheometer using a temperature sweep curve test in a cooling cycle. The viscosity gradually increases from 0.01 Pa s to 0.1 Pa s during cooling from 50 °C to 20 °C, respectively. A dramatic increase in viscosity occurs at temperatures below 20 °C, which is considered here to mark the start of solidification of the oil (Fig. 2). The magma analogue was mixed with red dye, which does not alter its viscosity, to provide a better visual contrast with the host material.

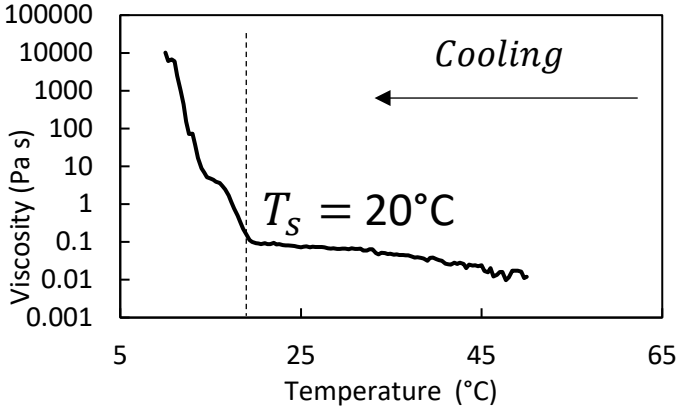

Figure 2. Dynamic viscosity of extra virgin coconut oil as a function of temperature. The vertical dotted line marks the estimated solidification temperature (i.e., T_s = 20 °C) of the oil used in the experiments reported here.

2.3. Scaling

Two dimensionless numbers have been adopted to scale and analyse the experiments reported here (Taisne and Tait, 2011; Currier and Marsh, 2015; Chanceaux and Menand, 2016; Arachchige et al., 2022). We also followed the scaling procedure for modelling analogue intrusions in Arachchige et al. (2022) and the key parameters in nature and their equivalent values in the experiments are summarised in Table 1.

The first dimensionless number is the dimensionless temperature, θ, which describes the thermal conditions of the experiments at the injection point (Table 1):

$$\theta = \frac{(T_s - T_g)}{(T_i - T_g)} \quad (1),$$

where T_s is the solidification temperature of the coconut oil (Fig. 2), T_g is the temperature of the host LRD gel before the injection, and T_i is the injection temperature of the coconut oil.

The second dimensionless number is the dimensionless flux, ϕ, defined as the ratio of the heat advected by the coconut oil to the heat lost by conduction into the host LRD gel. Assuming sills have axisymmetric geometry, where the length (L^2) and the area (S) are of the same order of magnitude (Chanceaux and Menand, 2016):

$$\phi = \frac{QH}{\kappa L^2} \quad (2),$$

where Q is the volumetric flow rate of injection, L is the horizontal length (or width) of the sill, H is the vertical thickness in the middle of the intrusion, and κ is the thermal diffusivity of the host material. Here, the thermal diffusivity of LRD is assumed to be the same as water, κ = 1.4

$\times 10^{-7}$ m^2 s^{-1} (Chanceaux and Menand, 2016). High values of ϕ indicate high injection rate and hence high heat flux into the system, which will tend to prevent solidification.

The initial dimensionless temperature, θ, was varied between ~0.1 and ~1 in the experiments by changing the injection temperature, T_i and the gel temperature, T_g (Table 2). As $\theta \rightarrow 1$, $T_i \sim T_s$ and solidification effects are expected to be relatively strong, while as $\theta \rightarrow 0$, $T_i >> T_s$ such that solidification effects should be relatively weak to negligible. The dimensionless flux ϕ varied from ~1 to ~60 in the experiments (Table 2). To ensure the experiments are properly scaled, θ and ϕ in the experiments must be similar to those in nature. Therefore, the values of the injection temperatures T_i and volumetric flow rate Q were chosen such that the corresponding experimental θ and ϕ values have a similar range to those expected for sills of basaltic magma composition (Chanceaux and Menand, 2016) in nature (Table 1).

2.4. Experiment analysis

The growth rate and the velocity of model intrusions over time are calculated by analysing images using ImageJ software. Since the propagating fronts of the intrusions are irregular, for each time step, we calculate best-fit circles to the magma-host rock contact to quantify horizontal sill growth rates. We use the radius of these best-fit circles to measure the average velocity of horizontal sill propagation; local velocity variations due to high degrees of marginal segmentation (i.e., lobes) in directions other than that of the primary flow are not considered here. After each experiment, solidified sills were carefully excavated from their LRD host material and immediately stored in a fridge for detailed examination and photography of their 3D morphology.

3. RESULTS

Ten experiments were performed with different initial coconut oil, T_i, and gel temperatures, T_g, and volumetric injection flow rates, Q (Table 2). In each experiment, a single

sill was emplaced in the interface between the two LRD layers by continuous injection of coconut oil. The resulting sills display a range of geometries and propagation styles depending on θ and ϕ (Figs. 3; Table 2).

3.1. Intrusion morphologies

We characterise three types of intrusion that formed based on whether they developed features that can be attributed to relatively weak ($\theta \rightarrow 0$, $\phi \rightarrow 60$), intermediate ($0 < \theta < 1$, $1 < \phi < 60$) or strong ($\theta \rightarrow 1$, $\phi \rightarrow 1$) solidification effects, described in detail below.

3.1.1. Intrusions with relatively weak solidification effects

Experiment 4 (Fig. 3a, $\theta = 0.25$, $\phi = 3.76$) is the type example of this intrusion behaviour, in which a penny-shaped crack with a smooth margin formed, and only patchy solidified areas developed on the top surface of the sill before the analogue magma erupted at the surface. Compared to the other experiments, such sills have larger surface areas and are relatively thin, being thickest at the centre of the intrusion. With time, these sills formed saucer-shaped intrusions (e.g., Exp. 2 and 5) with inner-to-outer sill transitions (Fig. 4). In plan-view, solidified coconut oil first appeared at the centre of the intrusion and then migrated towards the tip (Fig. 3a′). In cross-sectional view, solidified material was seen to be concentrated at the top and bottom contacts while the interior of the sill remained fluid.

3.1.2. Intrusions with intermediate solidification effects

Intrusions showing intermediate solidification effects did not form penny or saucer-shaped sills but developed elongate morphologies that lengthened parallel to the primary magma flow direction (i.e., sill long-axis). In comparison to intrusions with weak solidification effects, a striking morphological feature of this sill type was the presence of internal flow channels. Two examples of intrusions showing intermediate solidification effects but with different volumetric injection flow rates are compared below and in Figures 3b and c:

Experiment 10 (Fig. 3b, θ = 0.66, ϕ = 0.91): Compared to the weak solidification experiments, when the temperature of the gel was decreased to ~10 °C, for the same volumetric injection flow rate, sills with non-planar margins developed with internal channels, bounded by domains of solidified oil, that connected the leading edge of the sill to the magma injection point (i.e., needle tip, Fig. 3b″). In this experiment, solidification progressed from the thick centre to the thin outer rim of the sill. A long-lived internal channel, containing rafts of solidified analogue magma, split into a network of smaller channels towards the intrusion rim (i.e. break-out channels; Fig. 3b″).

Experiment 12 (Fig. 3c, θ = 0.66, ϕ = 7.63): Compared to Exp 10, the volumetric injection flow rate was increased from 1 ml/min to 5 ml/min. The intrusion was initially similar to the those formed in the relatively weak solidification experiments (Fig. 3a), forming a penny-shaped crack that solidified from the thick middle region to the thin outer margin of the sill. However, the solidification free propagating front was highly segmented and comprised finger-like and lobate structures. Unlike Exp 10, an obvious internal channel was not observed.

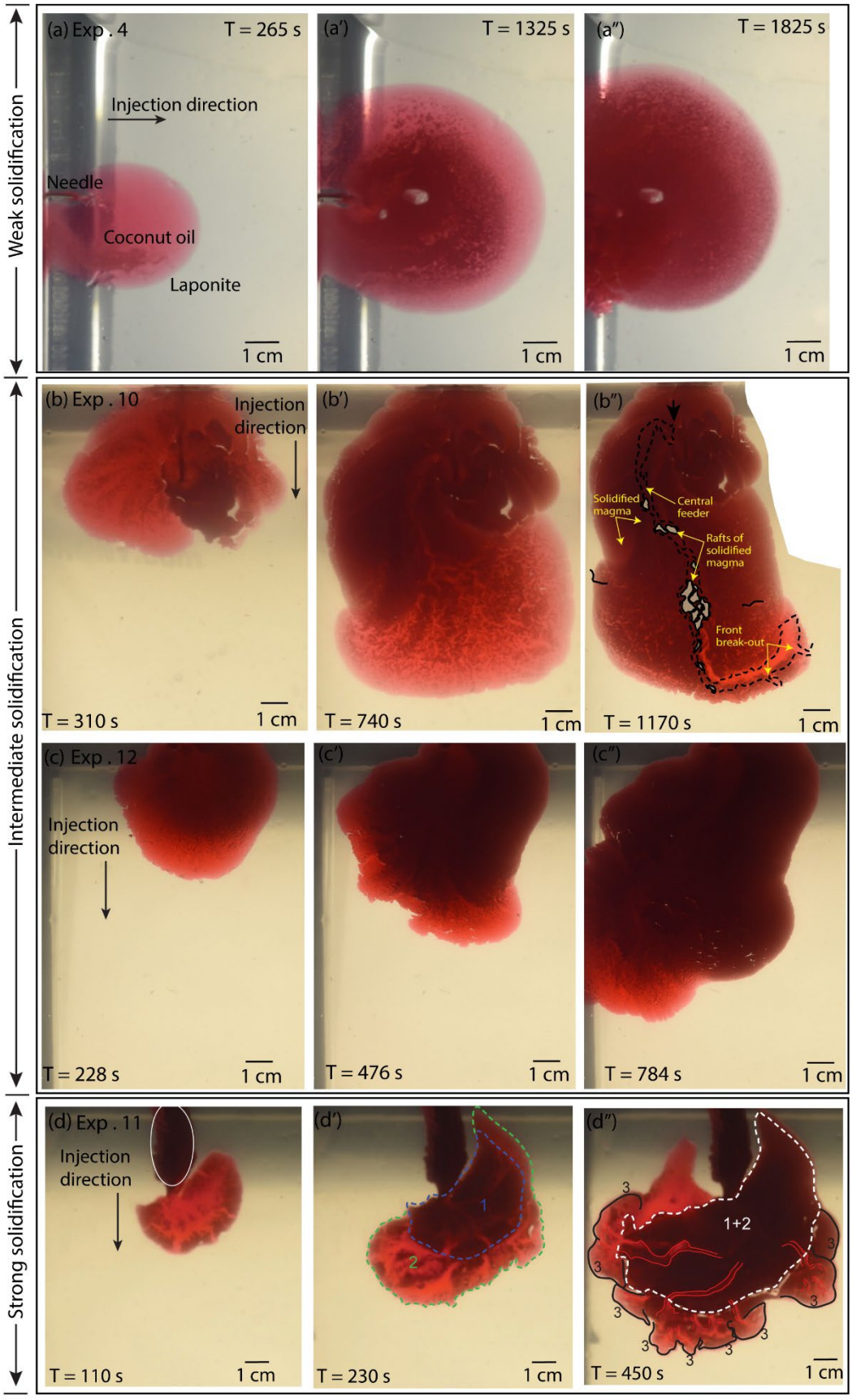
Weak solidification
(a) Exp . 4
T = 265 s
Injection direction
Needle
Coconut oil
Laponite
1 cm
(a′)
T = 1325 s
1 cm
(a″)
T = 1825 s
1 cm
Intermediate solidification
(b) Exp . 10
Injection direction
T = 310 s
1 cm
(b′)
T = 740 s
1 cm
(b″)
Solidified magma
Central feeder
Rafts of solidified magma
Front break-out
T = 1170 s
1 cm
(c) Exp . 12
Injection direction
T = 228 s
1 cm
(c′)
T = 476 s
1 cm
(c″)
T = 784 s
1 cm
Strong solidification
(d) Exp . 11
Injection direction
T = 110 s
1 cm
(d′)
1
2
T = 230 s
1 cm
(d″)
1+2
3
T = 450 s
1 cm

Figure 3. Plan views showing growth and morphologies of intrusions with relatively weak (a), intermediate (b, c) and strong (d) solidification effects. (a) In Exp 4. a smooth penny-shaped crack formed (θ = 0.25, ϕ =3.76, T_i = 25 °C, T_g = 18.2 °C, Q = 1 ml/min). In this experiment, solidification (dark red tones) progressed from the thick centre to the thin tip of the sill. (b) Exp 10. developed evolving solidification fronts with new lobes that led to the development of a non-planar intrusion margin and a long-lived internal flow channel that connected the central feeder to the rim of the sill (θ = 0.66, ϕ = 0.91, T_i = 25 °C, T_g = 10.2 °C, Q = 1 ml/min). In b′, a central feeder formed within the central part of the growing sill, and splits into channels that fed the tip of the sill. (c) Exp 12 had a higher magma injection flow rate compared to Exp 10 (θ = 0.66, ϕ = 7.63, T_i = 25 °C, T_g = 10.2 °C, Q = 5 ml/min). In this experiment, the sill front did not solidify (lighter red tones) during intrusion, only the central regions solidified. The intrusion margin is also strongly segmented with fingers and lobes and internal channelization is not observed. (d) Exp 11 (θ = 0.95, ϕ = 20.94, T_i = 20.5 °C, T_g = 10.3 °C, Q = 5 ml/min), has stronger solidification effects than Fig. 3b and c due to its higher value of θ and higher injection flow rate, ϕ. Solidification started at the propagating tip of the intrusion (darker patches at the rim of the sill), which then broke up into solidified blocks (d). The analogue magma subsequently opened up new lobe-like intrusion fronts that overtook the initial frozen sill margin (d′). Short-lived randomly oriented meandering channels (red lines) formed at a later stage and fed magma to the non-solidified propagating front (c). Numbers 1 to 3 outline the limit of the intrusion and its front (coloured dashed lines) at each step that the solidified margin was breached to form the next stage. The white elliptical line in (d) indicates the area of solidified analogue magma around the injection needle. For detailed model evolution, see Movies S1 (Exp. 4), S2 (Exp. 10), S3 (Exp. 12) and S4 (Exp. 11) in supporting information

3.1.3. Intrusions with relatively strong solidification effects

In experiments with relatively strong solidification effects (Exps. 11, 16; Fig. 3d, θ = 0.85 - 0.95, ϕ = 18.76 - 20.94), solidification occurred at the intrusion margins at early stages of emplacement, which resulted in complex intrusion geometries. Once formed, the solidified marginal material was subsequently disaggregated into solid blocks by inflow of new analogue magma during the formation of marginal lobes (Fig. 3d). Time-dependant, short-lived meandering internal channels were also observed. These sills formed in a discontinuous manner and propagated in pulses by discrete lobe growth, representing periods of momentary tip arrest due to freezing, followed by renewal of fracturing at the margins and growth of new lobes.

3.1.4. Nature and evolution of internal flow channels

Both long- and short-lived flow channels were observed in the experiments, depending on the degree of solidification. In experiments with intermediate solidification effects (e.g. Fig. 3b, Exp. 10), a flow channel became localised in the centre of the intrusion at an early stage (see Fig. 3b′ and b″). The orientation of this flow channel is subparallel to the primary flow direction of the incoming analogue magma. This long-lived flow channel initially began at the injection needle tip and terminated at the sill margin at a late stage of the experiment.

In contrast, short-lived flow channels were observed when solidification effects were relatively strong (Fig. 3d, Exp. 11). Unlike the long-lived channels, these channels neither connected to the injection needle tip, nor were they parallel to the primary flow direction in the sill. Compared to the long-lived flow channels, the length and duration of activity of these meandering flow channels were shorter. Short-lived flow channels originated close to transient solidified intrusion fronts within spaces created by breaking and/or disaggregation of frozen material (see Fig. 3d′ and d″). Their multi-directional orientation was therefore primarily controlled by breaks between solidified blocks of oil.

3.1.5. Excavated solidified sills

Post-experimental excavation of solidified sills from their LRD host material permitted detailed examination of their 3D morphology. Examples of excavated sills are shown in Figure 4. The sills in Figures 4a and b (Exps. 2 and 5) have saucer-shape morphologies with a flat inner sill and an inclined outer sheet and they also show segmentation into lobes at their outer margins. These features are similar to those formed in experiments in which no solidification occurred (Arachchige et al., 2022). Elongated and highly segmented intrusions formed in experiments with intermediate solidification effects (Fig. 4c). These intrusions also developed rough, groove-shaped upper surface structures, which formed in spaces between unsolidified oil that were filled with the LRD host material during the merger of lobe-like segments (Fig. 4e).

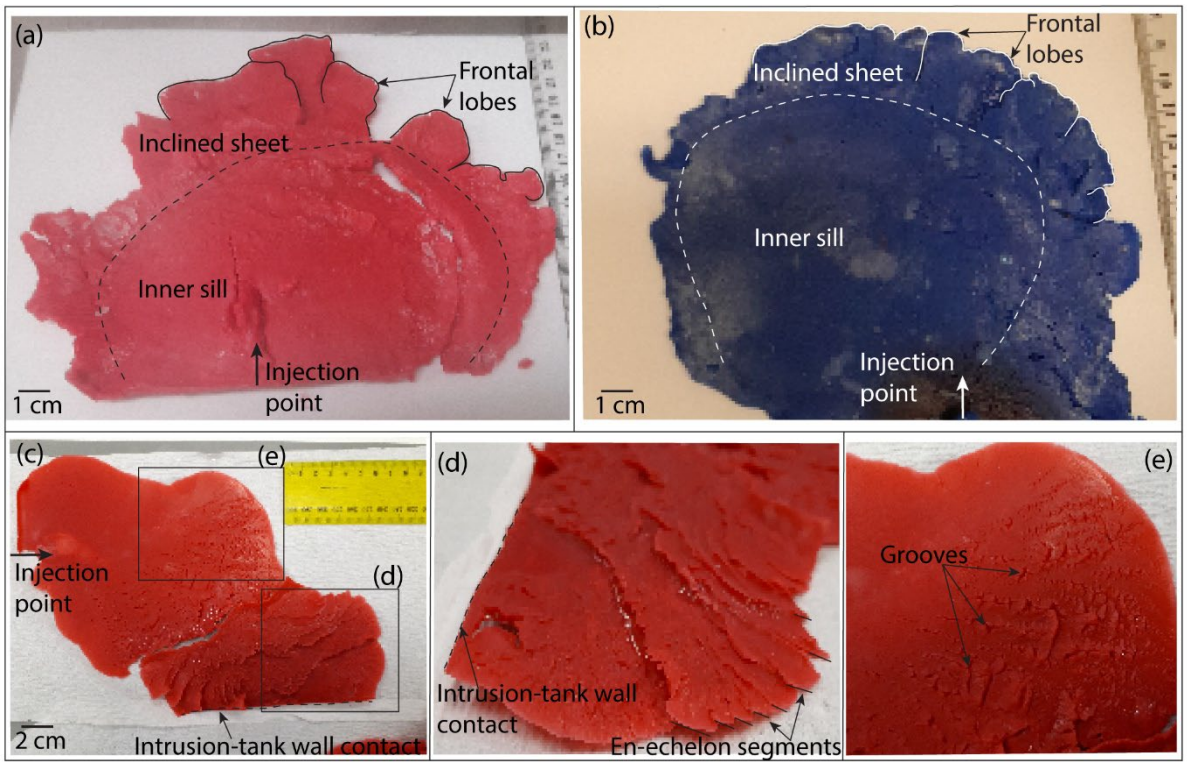

Figure 4. Morphology of intrusions after cooling and excavation from host LRD material. **(**a) Exp. 4 and (b) Exp. 2 with relatively weak solidification effects. Dotted lines mark the boundary between flat inner to inclined outer sill of these saucer-shaped sills. The inclined sheets that form the outer rim are highly segmented with frontal lobes. (c) Exp. 12, Elongate and highly segmented intrusion characterised by intermediate solidification effects . (d)

Closeup of (c) showing en-echelon marginal segments. (e) Closeup of (c) showing rough, groove-shaped features on the sill upper surface.

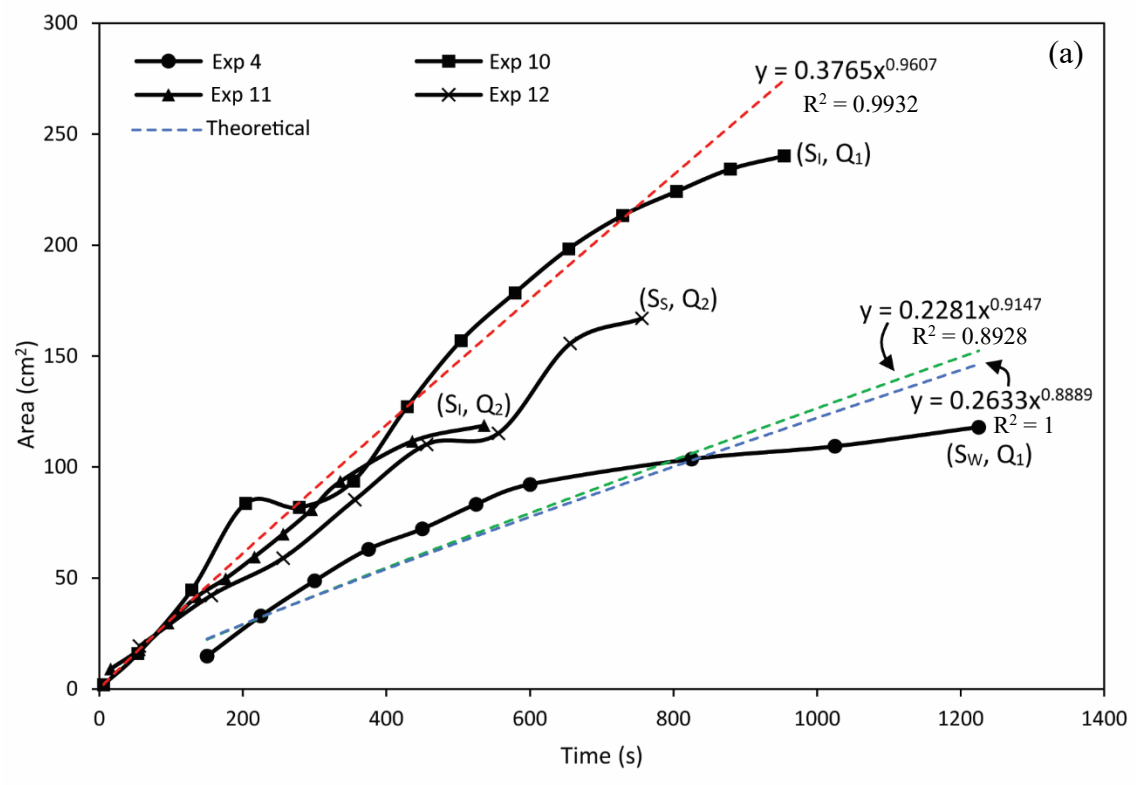

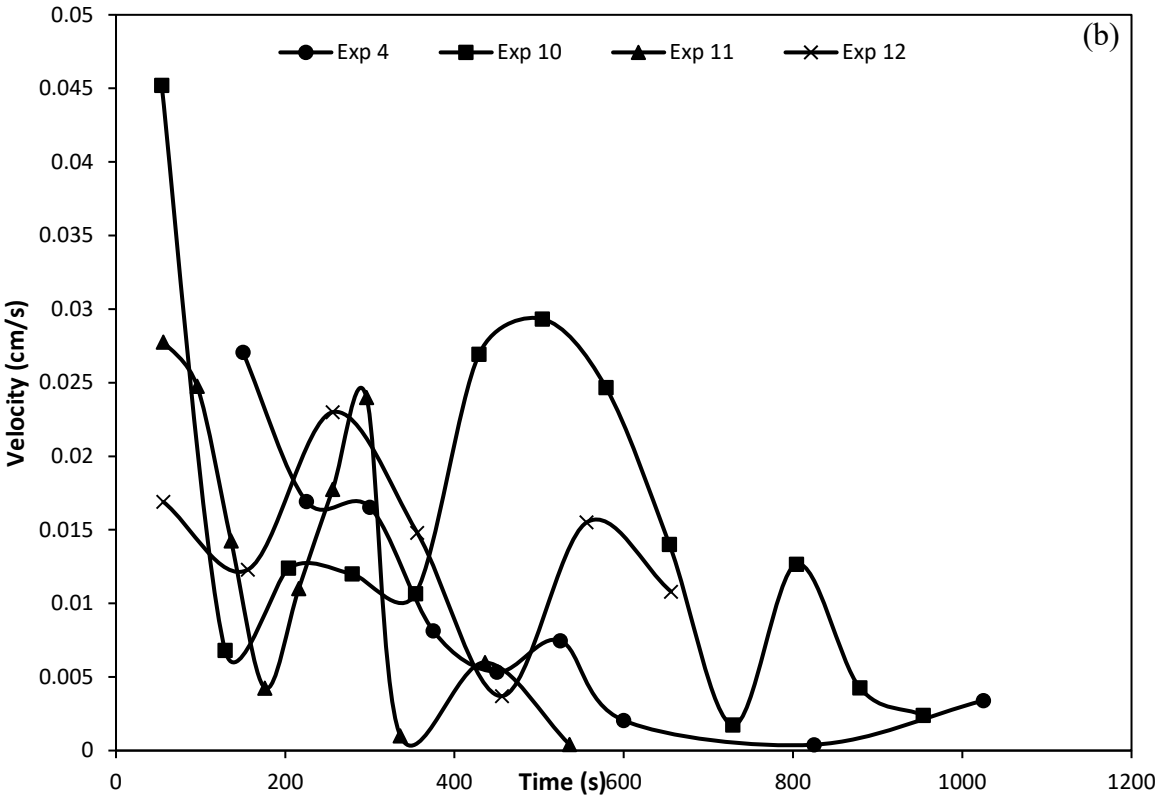

Figure 5. Area and average propagation velocity of intrusions in four selected experiments. (a) Intrusion area versus time. S_W – Weak , S_I – Intermediate and S_S – Strong solidification effects; Volumetric injection flow rates: Q_1 – Low (1.67×10^{-8} m^3 s^{-1}) and Q_2 – High (8.33×10^{-8} m^3 s-1). Dashed blue line shows the theoretical growth curve for a penny-shaped crack in an isothermal medium for the conditions equivalent to Exp. 4 and 10 (see text for details). Dashed green and red lines are the best-fit power-law curves for Exp. 4 and 10, respectively. (b) Average intrusion tip velocities were greatest at the beginning of each experiment, and then decreased with time in a fluctuating pattern.

3.2. Intrusion growth rates

Figure 5 plots the upper surface areas and the average tip velocities of intrusions against time for four experiments that represent the full range of solidification effects. The increase in surface area of the intrusions is almost linear up to 500 s, after which the growth curves start to flatten towards the end of the experiments. The highest and lowest growth rates were observed in Exp. 10 and 4, both of which had low injection rates and correspond to experiments showing relatively weak and intermediate solidification effects, respectively (Fig. 5a). Interestingly, Exps. 11 and 12, with higher volumetric injection rates, grew at similar rates that were between those of Exp. 10 and 4.

Fluctuations of the marginal propagation velocity (Fig. 5b) of the intrusions can be linked to transient periods of tip arrest followed by the opening of new propagation fronts, associated with the formation of new lobe segments. Average intrusion tip velocities vary significantly between experiments with relatively weak to strong solidification effects. In the weak solidification effect experiment (Exp. 4), the average tip velocity tended to decrease over time while also showing minor fluctuations. In experiments with intermediate solidification effects (Exp. 10 & 12), the amplitude of the total drop in tip velocity is higher than in

experiments with relatively weak (Exp. 4) or strong (Exp. 12) solidification effects and the magnitude of the velocity fluctuations is also greater.

4. DISCUSSION

4.1. Sill Morphology

A key observation from the experiments is that the final intrusion morphology appears to be controlled by the relative degree of solidification that occurred during its emplacement. Most experiments with relatively weak solidification effects produced penny-shaped or saucer-shaped intrusions with segmented inclined outer sheets (Fig. 3a) similar to previous isothermal experiments with no solidification (Arachchige et al., 2022). In contrast, intrusions that formed in experiments with intermediate to relatively strong solidification effects tended to be elongated with long- or short-lived internal magma channels (Figs. 3b, c, and d).

4.1.1 Experiments with weak solidification effects: comparison with previous experiments

Intrusions formed in experiments with relatively weak solidification effects had saucer-shaped geometries and segmented margins that resemble sills observed in nature (Chevallier and Woodford, 1999; Malthe-Sørenssen et al., 2004; Moy and Imber, 2009; Hansen, 2015; Reeves et al., 2018) and previous isothermal laboratory (Bunger et al., 2008; Mathieu et al., 2008; Galland et al., 2009b; Arachchige et al., 2022) and numerical modelling experiments (Haug et al., 2017; Walker and Gill, 2020). However, our results differ from previous laboratory experiments using solidifying magma analogues by Chanceaux and Menand (2016) and Currier and Marsh (2015), in which saucer-shaped sill morphologies did not form, despite them also displaying relatively weak solidification effects.

Chanceaux and Menand (2016) used layered visco-elastic gelatine as the host rock analogue and hot vegetable oil as magma analogue. In their experiments that showed relatively weak solidification effects, sills propagated continuously and had smooth upper surfaces. This contrasts with their experiments with relatively strong solidification effects in which sill

propagation occurred in a step-wise fashion with periods of transient arrest. Currier and Marsh (2015) modelled the effects of solidification during the growth of laccolithic intrusions using gelatine and either molten wax or water as the crustal and magma analogues, respectively. In their study, molten wax intrusions developed more complex morphologies with lobate margins compared to those using water as the magma analogue. In addition, water intrusions underwent smooth lateral expansion whereas molten wax intrusions did so in a strongly pulsating mode. However, none of the solidifying magma analogues in these experiments produced saucer-shaped sills, as observed in our experiments with relatively weak solidification effects. Our experiments used a crustal analogue with a complex visco-elasto-plastic rheology (i.e., Laponite RD® gel) (Arachchige et al., 2021) compared to brittle-elastic gelatine employed by Chanceaux and Menand (2016) and Currier and Marsh (2015) in their solidification experiments. Hence, we argue that the complex mechanical behaviour of the crustal analogue in our experiments with relatively weak solidification effects contributed to producing saucer-shaped sills with marginal segmentation during magma propagation and solidification.

4.1.2 Experiments with intermediate and strong solidification effects: elongate, pulsating intrusions with internal channels

Experiments with intermediate and relatively strong solidification effects produced elongated intrusion morphologies with lobe-like marginal segments that propagated in an intermittent or pulsating fashion (Exp 10, 11 & 12: Figs. 3, 5b). Importantly, these elongate intrusions often developed narrow, meandering tube-like channels that were long-lived in experiments with intermediate solidification effects and short-lived where solidification effects were strong. Using 3D reflection seismic reflection data, Miles and Cartwright (2010) identified a ~12 km long, narrow, meandering axial seismic amplitude anomaly within the central part of the elongate Vigra Sill Complex (Møre basin, North Sea), which they interpreted as a tube-like conduit that fed magma into the outer parts of the growing intrusion (Fig. 6a).

This linear feature resembles the meandering channels developed in our experiments with intermediate solidification effects (Fig. 6a and b).

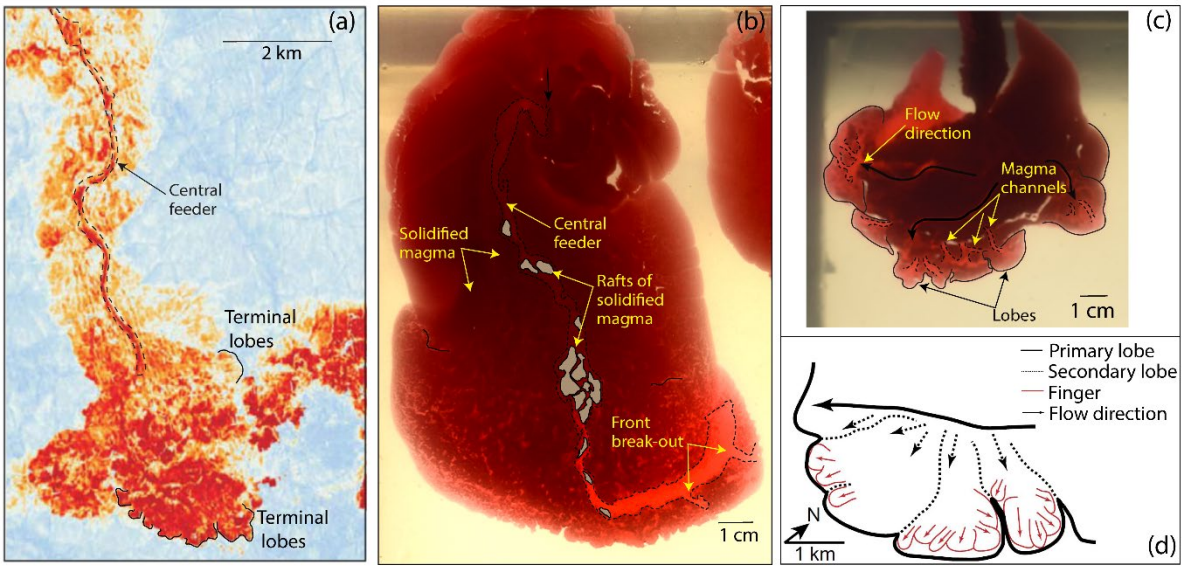

Figure 6. A comparison of magma Channelization and segmentation in nature and experiments**.** (a) Tube-like magma conduit in the Vigra Sill Complex (redrawn after Miles and Cartright (2010)). (b) Long, narrow channel in Exp. 10 with intermediate solidification effects (see Fig. 3b). (c) Short-lived, meandering channels formed in Exp. 11 with strong solidification effects (see Fig. 3d). (d) Magma lobes and fingers mapped in 3D seismic reflection data from a sill in the Rockall Trough (from Magee et al. (2015), modified after Thomson and Hutton (2004)).

4.2. Flow Channelization due to solidification versus pre-existing flow paths?

Here we discuss the styles and possible mechanisms of flow Channelization in igneous intrusions using the experimental results from this study and the literature. The geometry of the magma channels within solidifying sills in our experiments are similar to those observed from 3D seismic reflection studies (Thomson and Hutton, 2004; Miles and Cartwright, 2010). For example, 3D seismic reflection data analyses by Thomson and Hutton (2004) from the North Rockall Trough (compare Fig. 6c and d) indicate the presence of linear anomalies that have been interpreted as feeders of elongate, bilaterally symmetrical sill complexes with lobate geometries. Thomson and Hutton (2004) further showed that the North Rockall Trough sill has

primary and secondary flow directions, which fed primary and secondary lobes, respectively. Furthermore, 3D seismic reflection data analysis from NW Australia (Köpping et al, 2022) show similar results, in which first order elements (i.e., lobes and finger segments) contain second order elements representing primary and secondary flow directions, respectively.

We propose that the long- and short-lived meandering flow channels observed in our experiments form by different mechanisms. Long-lived flow channels are mostly parallel to the primary flow direction within the sill (see Fig. 3b′ and b″, see Movie S2 in supporting information). We suggest that they form due to thermal interaction between the hot, liquid magma analogue and the already solidified inner intrusion (i.e., they are thermally controlled). Thermal erosion due to continuous injection of high temperature analogue magma and internal circulation flow adjacent to newly solidified material may lead to the formation of persistent (i.e., long-lived) flow channels in our experiments. In contrast, short-lived meandering flow channels (see Fig. 3d″, see Movie S4 in supporting information) are relatively short and randomly oriented and appear to follow pre-existing flow paths (i.e., they are structurally controlled), which formed due to the breakage of solidified fronts mostly within lobes. Once a frozen intrusion tip breaks, a narrow channel is created into which the magma analogue flows to feed another flow front or lobe.

Although flow Channelization was not observed within previous experiments of solidifying sills, similar flow patterns have been documented in dyke ascent experiments using water or liquid gelatine and solid gelatine as the magma and crustal analogues, respectively (Kavanagh et al., 2018; Pansino et al., 2019). Kavanagh et al. (2018) showed that an internal circulation pattern develops within penny-shaped dykes comprising an upward central jet and lateral downward flow, forming a central channel. By injecting warm, liquid gelatine (magma analogue) into cold, solid gelatine (crustal analogue), Pansino et al. (2019) found that after a

dike erupts, it quickly channelizes into a centralised vent, transforming a long fissure eruption into a focused lava fountain.

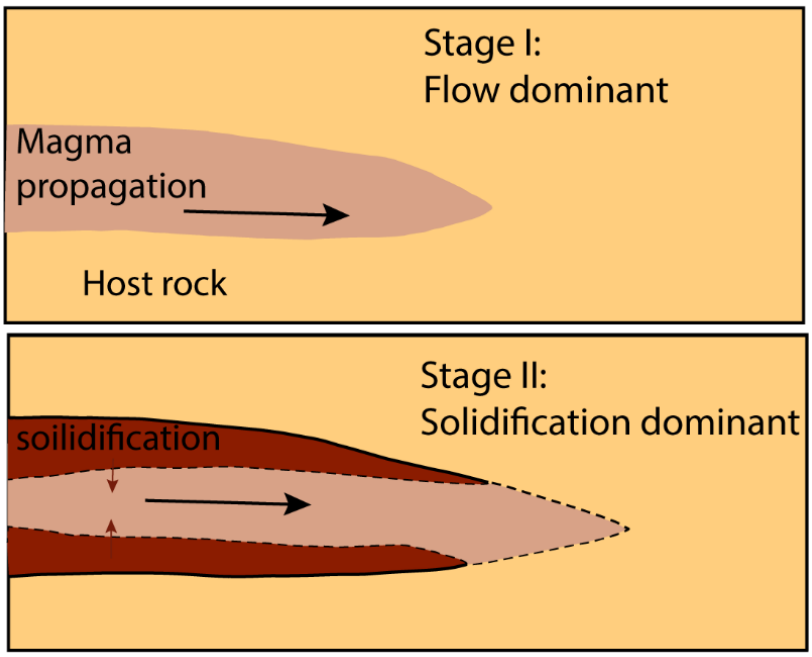

Figure 7. Cross sectional views of experimental intrusions with relatively weak and intermediate solidification effects. (a) Flow-dominated Stage I: a uniform crack propagates parallel to the primary magma flow direction while growing in length and width. (b) Solidification-dominated Stage II: Solidification first occurs at the top and bottom contacts between the host rock and the analogue magma except at the propagation tip. Red arrows in Figure. 7b show the inward movement of the marginal solidification fronts (i.e., thickened solidified volume), which eventually leads to channelization due to patches where the paths close up focusing the flow to high flow long-lived channels.

4.3. How solidification influences sill propagation dynamics

Here, we discuss possible solidification processes that may control the morphologies and emplacement dynamics of sills formed in the experiments reported.

For the same value of Q, the elongate sill that formed in Exp. 10 had almost double the area of the circular sill that formed in Exp. 4 at ~ 1000 s (Fig. 5a). However, Exp. 10 had the

greatest velocity fluctuations over time, which are linked to the opening of new, lobe-shaped propagation fronts. The best fit power-law curve ($y = 0.2281x^{0.9147}$) for Exp. 4 (dashed green line in Fig. 5a) is very similar to the theoretical curve ($y = 0.2633x^{0.889}$, dashed blue line in Fig. 5a) for an isothermal penny-shaped isothermal crack predicted by:

$$S = \left(\frac{Q^3 t^4 m}{12\eta}\right)^{\frac{2}{9}} \quad (3),$$

where Q is the volumetric flow rate, t is the time after the injection, η is the viscosity of the injected fluid and m is defined by:

$$m = \frac{E}{2(1-\nu^2)} \quad (4),$$

where E and ν are the young's modulus and the Poisson's ratio of the host rock, respectively (Chanceaux and Menand, 2016).

This finding indicates that the growth rate, morphology and the propagation style observed in this weak solidification experiment is similar to that expected for a non-solidifying, isothermal, penny-shaped crack.

We attribute the significantly greater areal growth rate of Exp. 10 ($y = 0.3765x^{0.9607}$) compared to both the theoretically predicted value and Exp. 4 to the propagation and solidification behaviour of this sill (strong tip velocity fluctuations and increased solidification effects). In this experiment, the injected fluid volume was mostly accommodated by creating new marginal lobes, resulting in a large surface area. Furthermore, the solidification along the upper and lower margins tended to supress vertical inflation, resulting in a thinner intrusion compared to Exp. 4. We suggest that the injected volume in Exp. 4 was accomodated within a thicker intrusion with a smaller area due to the absence of a segmented propagation margin and significant solidification along the upper and lower contacts. Interestingly, these results suggest that solidification promotes thinner intrusions with larger areas compared to equivalent isothemal sills.

4.4. Conceptual models for sill propagation patterns and solidification

We propose that the growth and solidification of sills in the relatively weak and intermediate solidification experiments can be described by a two-stage process (Fig. 7):

Flow-dominated Stage I: During this stage, solidification is absent and the fluid entering the sill from the feeder propagates outwards in a broadly radial pattern.

Solidification-dominated Stage II: At this stage, solidification occurs at the top and the bottom contacts of the intrusion but is absent close to the propagating front because of a combination of the time required to cool and solidify the injecting material when exposed to the cold gel at the tip (refer to Exps 2, 4 and 5; Fig. 3), and sill propagation is driven by unimpeded fluid flow as also observed in isothermal experiments (e.g., Arachchige et al., 2022).

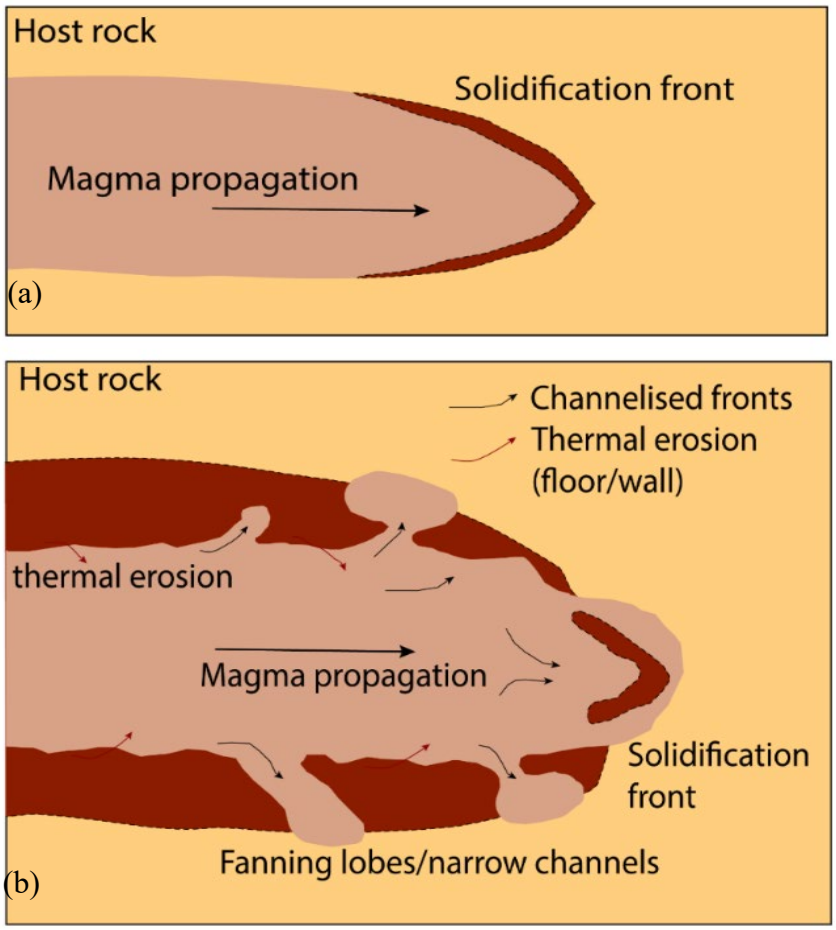

Figure 8. Interpreted cross sectional (a) and plan (b) view of Stages I and II, respectively, of intrusions with relatively strong solidification effects. The sill tip solidifies quickly, breaks and then splits due to continuous supply of analogue magma. Fluid then migrates into channels that follow breaks in the solidified front to eventually form new outward fanning lobes. This is associated with stalling and then renewed propagation of the sill tip.

In experiments with relatively strong solidification effects (i.e., Exp. 11, Fig. 3d), the growth and the solidification stages occur in the reverse order compared to experiments with relatively weak and intermediate solidification effects (Fig. 8):

Solidification-dominated Stage I: In contrast to experiments with relatively weak and intermediate solidification effects, solidification first occurs at the intrusion margin (Fig. 8a) (i.e., frontal solidification; Exp.11, Fig. 3d).

Flow- dominated Stage II: This stage is characterised by advancement of analogue magma via lobes (Fig. 8b). With continuing magma supply, the solidified front splits from the main intrusion (Fig. 3d′; Exp. 11). Such splitting allows magma to form a new intrusion margin comprising lobate segments. This new margin then solidifies and Stage 1 is abruptly repeated. Cyclic repetition between Stages I and II eventually creates narrow and meandering flow paths where the magma is allowed to channelize though the intrusion.

4. 5. Implications for channelized flow within sills

Our experimental observations have close similarities to channelized flow within sills in nature (Thomson and Hutton, 2004; Miles and Cartwright, 2010). Moreover, most studies of orthomagmatic Ni-Cu-PGE sulphide deposits (Seat et al., 2007; Saumur et al., 2015; Barnes et al., 2016) have suggested that a key requirement for ore deposition is prolonged and high-volume flow over a horizontal floor. Barnes et al. (2016) further showed that this floor may often take the form of a channelized sill or a tube-like intrusion (a.k.a., chonolith). They argue that if flow is short-lived, slow or intermittent, a single-phase intrusion will form with low

potential to develop ore bodies. Whereas longer flow channels, regardless of the flow rate, have strong potential to accumulate ore bodies. Therefore, the short and long-lived channels in our experiments have significant implications for understanding the internal dynamics of magma flow within sills and related intrusions in nature, including their potential to form economically important orthomagmatic ore deposits.

4. 6. A comparison with lava flows

There are close similarities between our experimental observations and lava flows. For example, Peterson et al. (1994) elucidated the development of lava lobes and tubes from observations from inflated pahoe-hoe flows on Kilauea, Hawaii. Such lava tubes have been explained in terms of the coalescence of lobes as they propagate, and thermal weakening of lobe walls. Moreover, lava tubes are similar to the channels imaged seismically within the Vigra Sill Complex (Miles and Cartwright, 2010). Fink and Griffiths (1990) observed folding and lobate structures in rapidly solidifying lava flows. Experimental work by Griffiths and Fink (1993) showed that for low extrusion and high cooling rates, flows advance by forming bulbous toes, lobes or pillows similar to those observed in natural pahoehoe and pillowed flows. At high extrusion and low cooling rates, pillowed flows turn into folded and leveed flows, which solidify only at their margins. Griffiths and Fink (1993) therefore showed that the formation of a solidified crust greatly impacts the morphology and internal dynamics of lava flows. Interestingly, this flow behaviour when cooling rates are high or low has parallels with our experiments with strong and intermediate solidification effects.

5. CONCLUSIONS

Our experimental findings illustrate the importance of solidification effects on the dynamics of sill emplacement into the upper crust, and highlight how this leads to different modes of magma flow channelization. The propagation dynamics and morphology of sills in our experiments depend strongly on their thermal evolution (dimensionless temperature and flux). When

solidification effects are relatively weak, sill propagation is continuous and forms penny-shaped intrusions which later turn into saucer-shaped sills. When solidification effects are intermediate to relatively strong, sills are elongated with complex morphologies, and they grow discontinuously in pulses by the formation of transient, discrete lobes. Importantly, sills formed in experiments with intermediate to relatively strong solidification effects developed two types of internal flow channels. Thermally controlled, long-lived channels form in intrusions in experiments with intermediate solidification effects, whereas structurally controlled, randomly oriented short-lived channels develop in experimental sills with relatively strong solidification effects. The lobate morphology and the development of flow channels in sills observed in the field and in 3D seismic reflection studies of sedimentary basins are consistent with the results of our experiments. We conclude that thermal conditions during syn-emplacement magma solidification play an important role in determining propagation mechanisms of sills and their final morphology. Furthermore, magma channelization within solidifying sills has significant implications for understanding of and exploration for intrusion-hosted, orthomagmatic Ni-Cu-PGE sulphide deposits.

ACKNOWLEDGEMENTS

The authors gratefully acknowledge support from an Australian Research Council Discovery Grant (DP190102422) to A.R.C. and a DIPRS and GRCA PhD scholarships from the Monash University (Melbourne) to U.S.N.A.

REFERENCES

Arachchige, U.N., Cruden, A.R., Weinberg, R., 2021. Laponite gels - visco-elasto-plastic analogues for geological laboratory modelling. Tectonophysics 805, 228773. https://doi.org/10.1016/j.tecto.2021.228773

Arachchige, U.N., Cruden, A.R., Weinberg, R., Slim, A., Köpping, J., 2022. Saucers , Fingers , and Lobes : New Insights on Sill Emplacement From Scaled Laboratory

Experiments Journal of Geophysical Research : Solid Earth. https://doi.org/10.1029/2022JB024421

Barnes, S.J., Cruden, A.R., Arndt, N., Saumur, B.M., 2016. The mineral system approach applied to magmatic Ni–Cu–PGE sulphide deposits. Ore Geology Reviews 76, 296–316. https://doi.org/10.1016/j.oregeorev.2015.06.012

Bertelsen, H.S., Rogers, B.D., Galland, O., Dumazer, G., Abbana Benanni, A., 2018. Laboratory Modeling of Coeval Brittle and Ductile Deformation During Magma Emplacement Into Viscoelastic Rocks. Frontiers in Earth Science 6. https://doi.org/10.3389/feart.2018.00199

Bolchover, P., Lister, J.R., 1999. The effect of solidification on fluid–driven fracture, with application to bladed dykes. Proceedings of the Royal Society of London. Series A: Mathematical, Physical and Engineering Sciences 455, 2389–2409. https://doi.org/10.1098/rspa.1999.0409

Bruce, P.M., Huppert, H.E., 1989. Thermal control of fissure eruptions. Nature 342, 665–667.

Bunger, A.P., Jeffrey, R.G., Detournay, E., 2008. Evolution and morphology of saucer-shaped sills in analogue experiments. Geological Society Special Publication 302, 109–120. https://doi.org/10.1144/SP302.8

Chanceaux, L., Menand, T., 2016. The effects of solidification on sill propagation dynamics and morphology. Earth and Planetary Science Letters 442, 39–50. https://doi.org/10.1016/j.epsl.2016.02.044

Chevallier, L., Woodford, A., 1999. Morpho-tectonics and mechanism of emplacement of the dolerite rings and sills of the western Karoo, South Africa. South African Journal of Geology 102, 43–54.

Currier, R.M., Marsh, B.D., 2015. Mapping real time growth of experimental laccoliths: The effect of solidification on the mechanics of magmatic intrusion. Journal of Volcanology and Geothermal Research 302, 211–224. https://doi.org/10.1016/j.jvolgeores.2015.07.009

Ernst, R.E., Head, J.W., Parfitt, E., Grosfils, E., Wilson, L., 1995. Giant radiating dyke swarms on Earth and Venus. Earth Science Reviews 39, 1–58. https://doi.org/10.1016/0012-8252(95)00017-5

Fink, J.H., Griffiths, R.W., 1990. Radial spreading of viscous-gravity currents with solidifying crust. Journal of Fluid Mechanics 221, 485–509. https://doi.org/10.1017/S0022112090003640

Fukushima, Y., Cayol, V., Durand, P., Massonnet, D., 2010. Evolution of magma conduits during the 1998-2000 eruptions of Piton de la Fournaise volcano, Réunion Island. Journal of Geophysical Research: Solid Earth 115, 1–21. https://doi.org/10.1029/2009JB007023

Galland, O., Planke, S., Neumann, E.R., Malthe-Sørenssen, A., 2009a. Experimental modelling of shallow magma emplacement: Application to saucer-shaped intrusions. Earth and Planetary Science Letters 277, 373–383. https://doi.org/10.1016/j.epsl.2008.11.003

Galland, O., Planke, S., Neumann, E.R., Malthe-Sørenssen, A., 2009b. Experimental modelling of shallow magma emplacement: Application to saucer-shaped intrusions. Earth and Planetary Science Letters 277, 373–383. https://doi.org/10.1016/j.epsl.2008.11.003

Griffiths, B.R.W., Fink, J.H., 1993. Effects of surface cooling on the spreading of lava flows and domes. 252.

Gudmundsson, A., 2011. Deflection of dykes into sills at discontinuities and magma-chamber formation. Tectonophysics 500, 50–64. https://doi.org/10.1016/j.tecto.2009.10.015

Hansen, D.M., Cartwright, J., 2006. Saucer-shaped sill with lobate morphology revealed by 3D seismic data: Implications for resolving a shallow-level sill emplacement mechanism. Journal of the Geological Society 163, 509–523. https://doi.org/10.1144/0016-764905-073

Hansen, J., 2015. A numerical approach to sill emplacement in isotropic media: Do saucer-shaped sills represent “natural” intrusive tendencies in the shallow crust? Tectonophysics 664, 125–138. https://doi.org/10.1016/j.tecto.2015.09.006

Haug, Ø.T., Galland, O., Souloumiac, P., Souche, A., Guldstrand, F., Schmiedel, T., 2017. Inelastic damage as a mechanical precursor for the emplacement of saucer-shaped intrusions. Geology 45, 1099–1102. https://doi.org/10.1130/G39361.1

Holness, M.B., Humphreys, C.S., 2003. The Traigh Bhan na Sgurra Sill, Isle of Mull: Flow Localization in a Major Magma Conduit. Journal of Petrology 44, 1961–1976. https://doi.org/10.1093/petrology/egg066

Jones, T.J., Llewellin, E.W., Houghton, B.F., Brown, R.J., Vye-Brown, C., 2017. Proximal lava drainage controls on basaltic fissure eruption dynamics. Bulletin of Volcanology 79, 81. https://doi.org/10.1007/s00445-017-1164-2

Kavanagh, J.L., Burns, A.J., Hilmi Hazim, S., Hignett, S., Wood, E.P., Martin, S.A., Dennis, D.J.C.C., 2018. Challenging dyke ascent models using novel laboratory experiments: Implications for reinterpreting evidence of magma ascent and volcanism. Journal of Volcanology and Geothermal Research 354, 87–101. https://doi.org/10.1016/j.jvolgeores.2018.01.002

Kavanagh, J.L., Menand, T., Daniels, K.A., 2013. Gelatine as a crustal analogue: Determining elastic properties for modelling magmatic intrusions. Tectonophysics 582, 101–111. https://doi.org/10.1016/j.tecto.2012.09.032

Kavanagh, J.L., Menand, T., Sparks, R.S.J., 2006. An experimental investigation of sill formation and propagation in layered elastic media. Earth and Planetary Science Letters 245, 799–813. https://doi.org/10.1016/j.epsl.2006.03.025

Köpping, J., Magee, C., Cruden, A.R., Jackson, C.A.L., Norcliffe, J.R., 2022. The building blocks of igneous sheet intrusions: Insights from 3-D seismic reflection data. Geosphere 18, 156–182. https://doi.org/10.1130/GES02390.1

Leslie, S.C., Moore, G.F., Morgan, J.K., 2004. Internal structure of Puna Ridge: evolution of the submarine East Rift Zone of Kilauea Volcano, Hawai`i. Journal of Volcanology and Geothermal Research 129, 237–259. https://doi.org/https://doi.org/10.1016/S0377-0273(03)00276-2

Lister, J.R., Dellar, P.J., 1996. Solidification of pressure-driven flow in a finite rigid channel with application to volcanic eruptions. Journal of Fluid Mechanics 323, 267–283. https://doi.org/10.1017/S0022112096000912

Lundgren, P., Poland, M., Miklius, A., Orr, T., Yun, S., Fielding, E., Liu, Z., Tanaka, A., Szeliga, W., Hensley, S., Owen, S., 2013. Evolution of dike opening during the March 2011 Kamoamoa fi ssure eruption , K ī lauea Volcano , Hawai ` i. 118, 897–914. https://doi.org/10.1002/jgrb.50108

Macdonald, R., BagińSki, B., Upton, B.G.J., Pinkerton, H., MacInnes, D.A., MacGillivray, J.C., 2010. The Mull Palaeogene dyke swarm: insights into the evolution of the Mull igneous centre and dyke-emplacement mechanisms. Mineralogical Magazine 74, 601–622. https://doi.org/10.1180/minmag.2010.074.4.601

Magee, C., Muirhead, J.D., Karvelas, A., Holford, S.P., Jackson, C.A.L., Bastow, I.D., Schofield, N., Stevenson, C.T.E., McLean, C., McCarthy, W., Shtukert, O., 2016a. Lateral magma flow in mafic sill complexes. Geosphere 12, 809–841. https://doi.org/10.1130/GES01256.1

Magee, C., Muirhead, J.D., Karvelas, A., Holford, S.P., Jackson, C.A.L., Bastow, I.D., Schofield, N., Stevenson, C.T.E., Mclean, C., Mccarthy, W., Shtukert, O., 2016b. Lateral magma flow in mafic sill complexes. Geosphere 12, 809–841. https://doi.org/10.1130/GES01256.1

Malthe-Sørenssen, Planke, A., Svensen, S.H., Jamtveit, B., 2004. Formation of saucer-shaped sills. Geological Society, London, Special Publications 234, 215–227.

Mathieu, L., van Wyk de Vries, B., Holohan, E.P., Troll, V.R., 2008. Dykes, cups, saucers and sills: Analogue experiments on magma intrusion into brittle rocks. Earth and Planetary Science Letters 271, 1–13. https://doi.org/10.1016/j.epsl.2008.02.020

Miles, A., Cartwright, J., 2010. Hybrid flow sills: A new mode of igneous sheet intrusion. Geology 38, 343–346. https://doi.org/10.1130/G30414.1

Moy, D.J., Imber, J., 2009. A critical analysis of the structure and tectonic significance of rift-oblique lineaments ('transfer zones') in the Mesozoic-Cenozoic succession of the Faroe-Shetland basin, NE Atlantic margin. Journal of the Geological Society 166, 831–844. https://doi.org/10.1144/0016-76492009-010

Muirhead, J.D., Airoldi, G., Rowland, J. V, White, J.D.L., Muirhead, J.D., Airoldi, G., Rowland, J. V, White, J.D.L., Mountain, T.C., Land, S.V., 2012. Interconnected sills and inclined sheet intrusions control shallow magma transport in the Ferrar large igneous province , Antarctica. https://doi.org/10.1130/B30455.1

Muirhead, J.D., Van Eaton, A.R., Re, G., White, J.D.L., Ort, M.H., 2016. Monogenetic volcanoes fed by interconnected dikes and sills in the Hopi Buttes volcanic field, Navajo Nation, USA. Bulletin of Volcanology 78, 1–16. https://doi.org/10.1007/s00445-016-1005-8

Norris, J., Giese, R.F., Costanzo, P.M., Vanoss, C.J., 1993. The Surface Energies of Cation Substituted Laponite. Clay Minerals 28, 1–11. https://doi.org/10.1180/claymin.1993.028.1.01

Pansino, S., Emadzadeh, A., Taisne, B., 2019. Dike channelization and solidification: time scale controls on the geometry and placement of magma migration pathways. Journal of Geophysical Research: Solid Earth 1–20. https://doi.org/10.1029/2019jb018191

Pollard, D., Delaney, P.T., Segall, P., 1982. Formation and interpretation of dilatant echelon cracks. Geological Society of America Bulletin 93, 1291–1303. https://doi.org/10.1130/0016-7606(1982)93<1291:faiode>2.0.co

Reeves, J., Magee, C., Jackson, C.A.L., 2018. Unravelling intrusion-induced forced fold kine- matics and ground deformation using 3D seismic reflection data. https://doi.org/https://doi .org/10.30909/vol.01.01.0117

Robertson, J.C., Kerr, R.C., 2012. Solidification dynamics in channeled viscoplastic lava flows. 117, 1–18. https://doi.org/10.1029/2012JB009163

Rubin, A.M., 1993. On the thermal viability of dukes leaving magma chambers. 20, 257–260.

Saumur, B.M., Cruden, A.R., Boutelier, D., 2015. Sulfide liquid entrainment by silicate magma: Implications for the dynamics and petrogenesis of magmatic sulfide deposits. Journal of Petrology 56, 2473–2490. https://doi.org/10.1093/petrology/egv080

Seat, Z., Beresford, S.W., Grguric, B.A., Waugh, R.S., Hronsky, J.M.A., Gee, M.A.M., Groves, D.I., Mathison, C.I., 2007. Architecture and emplacement of the Nebo-Babel gabbronorite-hosted magmatic Ni-Cu-PGE sulphide deposit, West Musgrave, Western Australia. Mineralium Deposita 42, 551–581. https://doi.org/10.1007/s00126-007-0123-9

Stasiuk, M. V, Jaupart, C., 1997. Lava flow shapes and dimensions as reflections of magma system conditions. 78, 2–4.

Taisne, B., Tait, S., 2011. Effect of solidification on a propagating dike. Journal of Geophysical Research: Solid Earth 116, 1–14. https://doi.org/10.1029/2009JB007058

Thomson, K., Hutton, D., 2004. Geometry and growth of sill complexes: Insights using 3D seismic from the North Rockall Trough. Bulletin of Volcanology 66, 364–375. https://doi.org/10.1007/s00445-003-0320-z

Tibaldi, A., 2015. Structure of volcano plumbing systems: A review of multi-parametric effects. Journal of Volcanology and Geothermal Research 298, 85–135. https://doi.org/10.1016/j.jvolgeores.2015.03.023

Walker, R.J., Gill, S.P.A., 2020. Tectonic stress controls saucer-shaped sill geometry and emplacement mechanism. Geology 48, 898–902. https://doi.org/10.1130/G47604.1